The characterization and effects of microstructure on the appearance of platelet-polymer composite coatings

C.M. SEUBERT[1, 2*], M.E. NICHOLS[1], J. FREY[1], M. SHTEIN[2] and M.D. THOULESS[2, 3]

[1]*Materials Research Department, Ford Motor Company, Dearborn, MI 48124, USA*
[2]*Department of Materials Science & Engineering, University of Michigan, Ann Arbor, MI 48109-2125, USA*
[3]*Department of Mechanical Engineering, University of Michigan, Ann Arbor, MI 48109-2125, USA*
[*]*Primary author contact: cseubert@ford.com, 313-322-3070*

Abstract

Although color and appearance have a psychological component, they are material properties that can be of considerable significance and economic importance to designers. Paint systems are materials that have a primary role of the modifying the appearance of an engineering structure. The determination of structure-property relationships is recognized as a defining feature for different branches of materials science. These relationships are at the heart of the predictive models required for the development of new materials. Here we explore some of the microstructural parameters that control the appearance of platelet-containing paint systems.

The orientation of platelets is a microstructural property known to affect the appearance of platelet-containing paints. However, prior works examined only a limited set of samples. Additionally, they did not identify other potential microstructural/formulation changes that could affect the relationship between orientation and appearance. In this paper, the orientation of the platelets was verified to be the major microstructural parameter that influenced the lightness of the paint system. In addition, the strength of this influence was shown to vary because of specific formulation changes, such as platelet size and volume fraction. The relationship between orientation and appearance was shown to depend on an additional microstructural property that is related to the size of the gaps between the platelets. We termed this additional microstructural property the *gap factor*. The size of the gaps between the platelets, and the coverage/shadowing of platelets by other platelets, was found to affect the scattering behavior of the system, particularly near the specular reflection direction. For example, larger gaps increase the probability of multiple reflections between the platelets. These results will guide on-going work to develop improved structure-property relationships. Improved structure-property relationships are expected to provide more accurate models for the appearance of platelet containing paint systems.

Keywords: Paint, color, scattering, metallic, flake, platelets

1. Introduction

Color, which is one component of appearance, can be thought of as a material property, which is important to humans for deep-seated, evolutionary reasons. It is, however, a property that is dependent on innumerable psychological biases, physiological factors, and environmental conditions [1,2]. Color is important for image recording and reproduction devices, surface finishing, and pigments; it is also an important consideration in the design of textiles, buildings, consumer products, and cars [3,4,5]. For example, in the automotive market, estimated to be worth $2 trillion dollars annually, 40% of buyers make purchasing decisions based primarily on the color of the vehicle [6]. Owing to this importance, attempts to quantify color and reduce it to engineering parameters that can be used in design are numerous, largely relying on empirical correlations [7,8,9,10]. However, from a materials science perspective, there is an important question of the extent to which such a property with a psychological component can be related to measurable microstructural parameters.

The appearance of a material or paint encompasses a number of properties that include gloss, texture, waviness and color. In this paper, we focus on color. Quantification of color is important for two reasons. First, a transformation to digital design is slowly taking place for color and appearance. Currently, this can only be done for simple colors, but there is a need for this process to evolve for the more complex colors associated with fabrics and automotive coatings. Second, the use of computational and combinatorial material design is rapidly progressing [11,12,13]. An enhanced understanding of the underlying physics and morphology that drive the color and appearance in complex materials will enable these techniques to be extended to the optical properties of materials.

Rendering of surfaces for visual modeling in computers relies on what is termed the bidirectional reflectance distribution function (BRDF). This is a function used to describe how the intensity of reflected light at a given angle of observation depends on the direction from which the surface is illuminated. The BRDF contains information about all aspects of a material's appearance. There are two extreme types of reflection. "Specular reflection" occurs from an optically smooth mirror, when the angle of reflection equals the angle of incidence. "Diffuse scattering" occurs when light is reflected from a perfect matte surface, and the intensity of the reflected light is equal in all directions. Generally, reflecting surfaces (including paint systems) exhibit a mixture of specular and diffuse reflections (**Figure 1**), leading to complicated forms of the BRDF [14,15] that depend on the details and microstructure of the reflecting surface.

The definition of color involves more than a simple measure of the wavelength or intensity of reflected light; there is a subjective aspect to color as well. Since it is useful to describe color in terms of quantifiable measurement specifications, the International Commission on Illumination (CIE) has developed standards to define color. These are quantified by a three-axis coordinate system of parameters that can be measured experimentally, and combined in a formula established by the standard. The coordinate system takes into account the features that induce physiological and psychological responses of the human eye and brain. The most commonly used system for paints is the "CIE1976 (LAB) color space" introduced in 1974 [7,8,9,10], which uses components of color described as the lightness (L^*), the green-red component (a^*) and the yellow-blue component (b^*). The development of new products in the paint industry typically focuses on how changes in the

composition or processing parameters affect the observed appearance through the use of CIE *L**, *a**, or *b** coordinates.

In the computer-graphics community, coatings are simulated by incorporating the BRDF (or a simplified model of it) into the rendering. These can be obtained by direct measurement of paint systems [16, 17]. Other approaches involve deriving a BRDF from models of primary ray scattering of the platelets [18,19,20,21,22,23]. However, experimental evidence to link these models to actual physical systems is lacking. The only work linking experimental observations of the platelets in an automotive paint to the resultant appearance is that presented by Sung [24] and Kettler [25], who explored the role of platelet orientation. In the present paper, we build on this earlier work by developing a more systematic investigation into how the platelet size, volume fraction, and spray conditions affect the appearance. This allows us to identify other microstructural properties beyond orientation that may play a role in the appearance of a metallic paint system, as a critical first step towards the creation of a direct link between formulation (processing), microstructure, and appearance (properties) in platelet-containing paint systems.

The paper is organized as follows. First, we review the main relevant advances in the science of color. Second, we present a model for the structure of the paint system under consideration, where metallic micro-platelet density and orientation affect light reflection. Third, we use this model to relate light scattering properties to the platelets' orientation, allowing for reverse-engineering of predicted microstructure from appearance. Finally, we compare the results of these predictions to the experimentally determined microstructures.

2. Microstructure of paint system

In this paper, automotive paints are used as a model system to explore appearance-microstructure relationships. Modern automotive paints are composite systems, containing pigments and metal platelets. The pigment particles range in size from 0.01 μm to 80 μm in diameter, and have a variety of shapes and crystal structures [26]. Metallic platelets with diameters between 1 and 80 μm, and thicknesses between 0.3 and 1.33 μm, were added to paint systems as early as 1935. At these thicknesses, no visible light is transmitted through the platelets that either absorb or reflect the light. Therefore, the surface platelets shadow the deeper ones. Metallic platelets produce variations in color and brightness with illumination and observation angles [27,28], and aluminum platelets are often used as the primary metallic pigment [27,29,30].

Physical attributes such as absorption spectra and refractive indices contribute to the appearance of a painted surface [31,32,33]. However, the microstructural characteristic thought to have the most significant effect on the appearance of paints is the distribution of the orientation angles of the platelets [27]. The arrangement of these platelets is determined by the processing conditions, such as how the paint is deposited on the substrate, and how it is cured [31]. An example of how these platelets are arranged in a 2-D cross sectional view of a standard automotive silver-paint system is shown in **Figure 2**.

Historically, the orientation of platelets within a polymer matrix has been measured using 2-D cross sections, similar to the one shown in **Figure 2** [28,34]. This technique is time consuming, and extracting a 3-D description of the distribution of the platelets requires

extensive stereographic analysis [35]. Other techniques, such as X-ray [36,37] and ion-microbeam analyses [38,39], are even more time consuming. Recently, researchers have begun to use laser-scanning confocal microscopy to create full 3-D representations of aluminum platelets, and to quantify orientation changes associated with different formulation and spray conditions [24,40]. This is the technique that will be used in this study to characterize the microstructure of the paints.

While LSCM provides a technique to obtain the 3-D distributions of platelets, there has been only a limited amount of work done to determine if an accurate description of the platelet orientation distribution can be extracted from scattering data for a complete system [24]. In that previous work, differences between the predicted and measured scattering profile were attributed to the platelet's surface roughness, which led to a wider specular reflection lobe from the platelet's surface. If it could be shown that the orientation distribution and the scattering profile are closely linked, then the orientation of the platelets could be determined by scattering measurements, rather than by the more-involved microscopy studies. Simpler micro-facet models for these systems could also be employed if this were the case.

3. Model for color

In this paper, we determine color by measuring gonioapparent scattering profiles, which constitute the distribution of scattered light over all possible viewing angles. The easiest measure of color that can be extracted from this is the lightness value, L^*, which can be calculated from [41]

$$L^* = 116\,(Y/Y_n)^{1/3} - 16 \qquad (1)$$

where Y is the measured intensity of the light reflected from the sample, and Y_n is the intensity of light that would be reflected at the same angle from a perfectly diffuse white reflector, while the constants and the exponent are empirically determined. In applications where a light source with a range of wavelengths is used, Y and Y_n are one of the tristimulus values for both the sample and the diffuse white standard [42,43]. However, in our experiments, a single wavelength is used, so a simple ratio of the intensity response is sufficient to calculate the lightness. A difference of magnitude one in the lightness corresponds to about the resolution limit that the human eye can detect in metallic paint systems [26].

The relationship between scattering and microstructure in these paint systems can be modeled assuming that the majority of scattering events occur as the result of single-reflection events (no multiple reflections). If the incident light comes from a single angle, the intensity of scattered light at a given angle of observation, θ_{OUT}, is directly related to the surface area of platelets at different orientations. A schematic illustration of such a single-reflection event is shown in **Figure 3**.

To relate the incident and exit angles for a given platelet correctly, refraction at the clearcoat/air interface must be accounted for. As the index of refraction of the polymer matrix (typically ~1.5) [44] is greater than that of air, the angle of incidence of any light that interacts with the system will change at the polymer/air interface (in this case, the top of the clearcoat layer). From Snell's law, the incident angle for a given flake can be expressed as

$$\theta_2 = \sin^{-1}\left({}^{1}/_{1.5}\sin\theta_{IN}\right), \tag{2}$$

where θ_2 is the incident angle after refraction, θ_{IN} is the initial angle of incidence with respect to the clearcoat surface, with the refractive indices for air and the clearcoat being 1 and 1.5, respectively. For the experiments that are described later, the angle of incidence is θ_{IN} = 45° and, therefore, θ_2 = 28°. After the incident light is reflected from the platelets, it is refracted again at the surface of the clearcoat. The exit angle for the reflected light, θ_{OUT}, is then given by

$$\theta_{OUT} = \sin^{-1}(1.5\sin(\sin^{-1}(\,{}^{1}\!/_{1.5}\sin\theta_{IN}) - 2\theta_F) \quad , \tag{3}$$

where θ_F is the angle of orientation for the platelet orientation angle. If it is assumed that the platelets all have the same size, the predicted intensity of light in a particular direction then depends on the distribution of orientation angles for the platelets. From this, the lightness, L^*, can be computed using Eqn. (1).

4. Experiments & Results

4.1 Materials

A set of automotive basecoat/clearcoat acrylic paint systems with varying platelet sizes, volume fractions and application conditions was studied. Thus, a comparison between scattering and morphology could be made across a larger scope of samples than has previously been done [24]. Samples were prepared using standard automotive coating techniques, with specific details listed in **Table 1.** The target thickness of the basecoat layer was 20 μm. The basecoat layer was flash dried at ambient conditions to allow for solvent evaporation, before the acrylic clearcoat layer, with a target thickness of 50 μm, was applied. The samples were cured in a convection oven for 20 minutes at 130°C.

Images of the finished samples were taken at 15° off-specular (OS) under daylight illumination provided by a MacBeth light booth (X-Rite Inc., Grand Rapids, MI USA). These images are shown in **Figure 4.**

The systems identified as "Silver #1" through "Silver #3" were silver formulations, sprayed to hiding (minimal transmission) with a rotary bell applicator onto steel panels that had been previously coated with a grey automotive primer. The same basecoat and clearcoat formulations were applied to all three samples, but they were sprayed at different flow rates. The droplet size becomes more variable as the flow rate is increased, resulting in less control over the deposition of the droplets, which is thought to result in more disoriented platelets before curing [45,46].

The systems identified as Silver #4 through Silver #6 were also formulated to prevent light transmission through basecoat layer. Each was formulated with a different size platelet, ranging in diameter from 11.5-25 μm (**Table 1**). All three basecoats and the clearcoats were applied to steel panels that had been previously coated with a grey automotive primer.

The systems identified as "Silver #7" through "Silver #10" were formulated from the same initial composition (Silver #7), but the platelet concentration was progressively reduced by diluting Silver #8 through Silver #10 with unpigmented resin. The coatings were manually applied with a high-volume low-pressure (HVLP) spray gun to primed steel panels. The clearcoat layer was applied with a drawdown bar (a device used to manually draw a wet film over a substrate at a constant thickness) after the basecoat was cured. These systems were deposited on a black automotive primer (to eliminate reflection off of the primer layer in the

non-hiding formulations), but had the same target thickness of 20 μm for the basecoat and 50 μm for the clearcoat.

4.2 Characterization of Microstructure

Direct measurements of the platelet/polymer composite microstructures were accomplished using Laser Scanning Confocal Microscopy (LSCM). This technique allowed for the creation of platelet orientation distributions for each of the analyzed systems. LSCM images were acquired using a Zeiss LSM 5 Pascal LSCM (Thornwood, NY) configured on a Zeiss Axioskop 2 upright microscope. LSCM uses a laser light source and collects the reflected light within the focal plane of the measurement. (Light outside the focal plane is rejected.) The focal plane is moved step-wise through the sample thickness to collect a series of images, which can later be combined into a 3D image of the entire sample. The series of confocal reflected-light images were acquired using the 488 nm Argon gas laser line, viewing through the top thickness of about 20 μm of the basecoat in 0.25 μm steps, with a 40x Plan-Neofluar oil objective (NA 1.3). Topographic analyses were performed on the confocal image series using the Zeiss LSM 5 Pascal Topography software. MountainsMap surface-analysis software from Digital Surf (Besançon, France) was used to calculate the area, normal, and azimuthal angle of each visible platelet. The normal angle is the planer angle between the vector perpendicular to the clearcoat surface and the vector perpendicular to the platelet's face (0^o – 90^o). The azimuthal angle is the spherical angle of the vector perpendicular to the platelet's face (0^o – 360^o). Typically, 5 to 6 distinct regions were measured to collect data from a statistically significant number of platelets (400-500), so that the orientation distribution across from each system was reliably obtained.

LSCM images were obtained for each of the ten samples at multiple locations on each panel. An example of a height map for Silver #1 is shown in **Figure 5.** One specific advantage of LSCM measurements, as opposed to 2D cross-sectional measurements, is that the LSCM only images the platelets (partial and full) that are immediately observable by incident light. These particular platelets are the ones that directly affect the appearance that is the primary focus of this study. Platelets deeper within the system that are completely covered by surface platelets do not contribute as directly to the appearance. Data for the normal and azimuthal angles were measured for each visible platelet using the height maps. The absence of any obvious azimuthal orientation of the platelets confirmed a random distribution in that direction. This is shown for the Silver #1 data in **Figure 6A**. As the azimuthal angles were random, only the normal angles of the platelets were considered to be of consequence; these were the only angles considered in the rest of this work.

The distribution of normal angles for the orientation of the platelets (θ_F) was measured from the LSCM images. An example of the raw data is shown in **Figure 6B** for Silver #1. These frequency data were then integrated and normalized to a total value of 1.0 to produce the cumulative-distribution functions (CDFs) for each sample. To provide a point of comparison for these data, hypothetical examples of the CDFs corresponding to the system with (i) a perfectly parallel orientation, (ii) a good orientation, (iii) a poor orientation, and (iv) a perfectly random orientation are shown in **Figure 7.** The CDFs for the three sets of paints are shown in **Figure 7B-D**. In these plots, the angles for all the platelets were weighted equally, and were not adjusted for size of the platelets.

4.3 Prediction of microstructure from scattering data

The appearances of the different systems were measured using scattering experiments in which the samples were illuminated at a given angle of incidence, with the scattered light being collected at specific angles of observation. The scattered intensities were measured using a Radiant Zemax IS-SA Imaging Sphere (Redmond, WA). The IS-SA Sphere uses a hemispherical mirror to measure 2π steradians of scattered light at one time. The collimated incident light was produced by a xenon light source that illuminated a 20 mm diameter circular region from which the scattering data were obtained. The measurements were taken at a wavelength of 555 nm. The angular resolution of the measurements was 0.5^{o}. A single scattering profile of each sample was determined by illuminating the sample at 45^{o} from the normal, and measuring the scattered intensity across the hemisphere. An example of the resulting spherical contour plot of the scattered intensity for Silver #1 is shown in **Figure 8**. The lightness values, L^{*}, for each sample 15^{o} OS ($\theta_{OUT} = 30^{o}$) were calculated from Eqn. (1) and are tabulated in **Table 1.**

The scattering profiles obtained for the different paint systems can be used to deduce the distribution of the orientation of the platelets, by re-arranging Eq. (3):

$$\theta_F = 0.5 * [\sin^{-1}(1/_{1.5} \sin\theta_{IN}) - \sin^{-1}(1/_{1.5} \sin\theta_{OUT})] \quad (4)$$

where θ_F is the platelet orientation angle, θ_{OUT} is the flux angle after it exits the clearcoat layer, and $\theta_{IN} = 45^{o}$.

It should be noted that the scattering measurements were made in units of inverse steradians. Therefore, in order to eliminate the effect of the solid angle upon this measured

intensity, and to convert the scattered data to values directly proportional to platelet angle area/frequency, the scattering intensities were normalized to that of a perfectly diffuse white scatterer. This normalization results in the relative area of platelets oriented at a particular angle. From the frequency data of these relative areas, CDFs for the orientation of the platelets were calculated. Furthermore, the setup of the scattering measurement resulted in a blind spot at the source of the incident light (at 45^{o} to the normal). As a result, all the calculations for the orientation of the platelets were made from scattered light collected between the direction of the incident light source and the direction of the specular reflection.

The CDFs of the platelet orientations from the different paint systems, as determined by confocal microscopy, are plotted in **Figure 9a-j.** Superimposed on these plots are the corresponding CDFs predicted from the scattering data**.** Silver #7 was the most oriented system, with a median orientation angle of 3.1 ± 0.2^{o} (based on the LSCM data)**.** Silver #10 was the least oriented system, with a median orientation angle of 7.0 ± 0.4^{o} (based on the LSCM data).

5. Discussion

5.1 Relationship between measured and predicted orientations

The strength of the orientation-scattering link between the two measurements can be described by the difference between the orientation curves obtained by the two techniques. Qualitatively, one can see from **Figure 9** that the orientations obtained from microscopy and from the scattering analyses are similar for Silver #4; they are less so for Silver #6. To quantify

the degree of agreement, the root-mean-square (RMS) error between the microscopy and scattering orientation curves was calculated and summed for each sample using the equation

$$RMS_{error} = \sqrt{\sum (X_M - X_S)^2 / n} \quad (5)$$

where X_M and X_S are corresponding points on the orientation curves calculated from the microscopy and scattering measurements, and *n* is the number of points analyzed. The results of this calculation are listed for each sample in **Table 1.**

To determine if the platelet angles should have been weighted based on the visible area of each platelet, weighted platelet distributions (w-LSCM) were calculated and plotted for Silver #4-Silver #6 in **Figure 9d-f**. The frequency of the orientation angle for each platelet was scaled by the visible area of the platelet to produce a weighted CDF. The visible area of an individual platelet is the area directly viewable by LSCM and not shadowed by other platelets. Therefore, platelets with large visible areas are expected to have a greater effect on scattering and on lightness than platelets with smaller visible areas. This visible area was measured from LSCM scans, as illustrated in the call-out of **Figure 5**. As shown in **Figure 9**, these weighted distributions did not result in a better agreement with the predictions from the scattering distributions.

The strength of the relationship between orientation and scattering is shown to vary as a result of formulations changes (**Figure 9).** Three effects have been considered to explain the discrepancies between the orientation profiles measured by microscopy and those deduced from scattering measurements. These effects are (i) reflections from the edges of samples, (ii)

scattering from rough surfaces, and (iii) multiple reflections between platelets, considered in more detail below.

5.2 Edge Reflections

Reflections from the edge of the platelets, as shown schematically in **Figure 10a**, is one possible reason why there is a discrepancy between the measured and deduced orientations. This type of reflection will be manifested primarily in the backscattered region. An increase in thickness would result in additional reflections from the edges of the platelets. This would affect the interpretation of the scattering data, but would not contribute to the measurements of the orientation distribution from the LSCM experiments. Therefore, the associated RMS_{error} values would be expected to increase for thicker platelets. Furthermore, the two distributions would be expected to be well-matched at small orientation angles, and to deviate only at larger angles (greater than 10^{o} to 15^{o}). As shown by the curves of **Figure 9**, the data do not follow either of these patterns. Therefore, edge reflections do not appear to be the reason for discrepancies between the structure-property relationships.

5.3 Surface Roughness

The surface roughness of the platelets is a second possible cause for the discrepancies between the measured and predicted distributions. The surface roughness of the platelets was measured from platelets filtered out of the appropriate basecoats. The liquid paint was dissolved in methylene chloride, and then the mixture was passed through Grade 2 filter paper. A Wyko NT3300 (Bruker Corp., Billerica, MA), non-contacting, white-light interferometer was used to quantify the surface roughness of the platelets that were deposited on the filter paper.

The resultant root-mean square roughness was determined to be 51.4 ± 10.0 nm, with no systematic difference being observed between the roughness values of the platelets from different paints.

The Raleigh criterion for the maximum roughness, *H*, that a surface can have if it is to be considered to be optically smooth is given by [47]

$$H < \frac{\lambda}{8 \sin \beta} \quad (6)$$

where, λ is the wavelength of incident light, and β is the angle of incident light. This limiting value is about 70 to 115 nm for the illumination conditions of the experiments. This is on the order of the root-mean square roughness of the platelets, which was ~51.4 ± 10.0 nm, as discussed above. This indicates that the scattering from a platelet face should be focused in the specular direction, but also may exhibit some broadening of the specular lobe. The exact shape of the reflectance lobe from individual platelets is currently being investigated by computer simulation, and will be reported in a future manuscript.

5.4 Multiple Reflections

Multiple reflections between the surfaces of platelets are possible if light passes through a space in the top layer of platelets and is subsequently reflected from a deeper platelet to hit the bottom surface of another platelet (**Figure 10b**). For visible wavelengths, absorption associated with each reflection results in a reduction of the intensity by approximately 8% [48]. These internal reflections will also affect the effective angle of reflection, but numerical simulations would be required to obtain relationships between the angle of incidence and the angle of reflection, since the number of reflections that a particular

ray may experience is not known *a priori*. In this section, we address two microstructural features that affect multiple reflections: (i) the height, or gap, between platelets in different layers (**Figure 10**), and (ii) the *coverage* - the degree to which platelets are obscured or shadowed by other platelets.

5.4.1 Gap Factor

To determine the effect of gaps upon the scattering behavior, an analysis of the gaps between the platelets was performed using the same LSCM scans that had been employed for measuring the orientations. Line scans provided topographical profiles of the topmost platelets. An example (from Silver #1) is shown in **Figure 11**.

The large height changes are associated with gaps between platelets, while the smaller height differences are associated with local, intra-platelet topographical changes. Small fluctuations in the height were filtered out by calculating the derivative of the height with respect to distance, and eliminating peaks associated with slopes having magnitudes of less than one. The remaining peaks in the derivative profile, which are assumed to be associated with gaps between the platelet upper surfaces, were integrated and summed over the entire profile. The resulting sum is the cumulative gap over the length of the scan. This quantity was normalized by dividing it by the scan length to produce what is termed the "gap factor" for the system. A larger gap factor provides a greater opportunity for light to penetrate below the top layer of platelets, and to undergo multiple reflections, be it off edges or platelets below the surface. The results from ten to twelve line scans were averaged for each of the ten silver paint systems, and the resultant "gap factors" are reported in **Table 1.**

As shown in **Figure 12,** a moderate correlation may exist between the gap factor and the RMS_{error}, if the gap factor is greater than about 0.15. The single datum that doesn't seem to fit with the other data is the result from Silver #7. This is a system that was sprayed by hand to complete visible hiding. It exhibited the highest degree of orientation (**Figure 9g),** and the lowest gap factor out of all the samples tested. For this sample, the scattering must be dominated by primary reflections, since opportunities for multiple reflections are few. Therefore, in this system, broadening of the scattering data is caused primarily by the roughness of the platelets and by reflections from the edges of platelets. On-going work is being done to establish whether this single point indicates a break down in any possible correlation between gap factor and RMS_{error} at low gap factors, or whether it represents a change in the relationship. This study requires the careful preparation of systems with good orientation and low gap factors, which we did not fabricate in this initial study.

Figure 13 shows that when systems with similar orientation profiles are compared, Silver #4 through Silver #6, there appears to be quite a strong linear correlation between the gap factor and the RMS_{error}. This possible connection between orientation distributions and scattering behavior will be explored in the future, using controlled simulations of these paint systems, in which the effect of each contributing factor can be considered independently.

The three samples identified as Silver #4 through Silver #6 possess very similar platelet orientation distributions (**Figure 7c**), yet their lightness values at 15^{o} OS are significantly different, as detailed in **Table 1**. The only significant difference between the three samples is the gap factor. The relationship between the lightness at 15^{o} OS and the gap factor is shown in

Figure 14 for the three samples. This illustrates that the size of the gaps between the platelets may be an additional microstructural component that contributes to the color of a material. Larger gaps may result in more secondary reflections; the multiple reflections will result in more light being scattered away from the macroscopic specular direction.

5.4.2 Coverage

Another microstructural feature related to the density of the platelets and the gaps between them is what we will call "fractional coverage" -- the degree to which platelets are obscured or shadowed by other platelets. For example, a platelet that is completely obscured by other platelets is described as exhibiting a fractional coverage of 1.0, while a platelet on the surface of the basecoat layer will have a fractional coverage of 0.0.

To examine the effect of coverage, a pair-correlation microstructural analysis was employed to determine if specific morphologies affected the directional distribution of the scattered light in these systems. The pair-correlation function (also known as the radial-distribution function) is a technique used in statistical mechanics. It describes the density of a system of particles by measuring the distance between particle centers [49,50,51,52]. Here, the technique was modified to analyze 2D cross sections, similar to that shown in **Figure 2**, and it was used to describe the microstructure of the paint systems.

The center of each platelet was identified, and used as a reference point. From that center point, rays were projected towards the surface at 5° increments (**Figure 15**). The percentage of rays emanating from the center of the upward-facing surface of a platelet that intersect another platelet was defined as the coverage of a platelet, C_v. Conversely, the

probability that light entering the system from any direction will have a primary reflection off a platelet is assumed to be given by 1-C_v (ignoring the finite size of the platelets).

For a multiple reflection event to occur from a particular platelet, light must reach that platelet, and the reflection must strike a second platelet. The probability of both of these events happening, P_m, for light entering from any direction is

$$P_m = C_V(1 - C_V) \tag{7}$$

This probability has a maximum of 0.25 when C_v is equal to 0.5. So, platelets with a fractional coverage of between 0.25 and 0.75 are the most likely to cause multiple reflections.

The form of Eqn. (8) implies that if a composite paint system is illuminated across all angles (diffuse illumination), a quick transition from platelets with zero coverage to complete coverage as a function of depth will result in a lower incidence of multiple reflections. To examine this prediction, the coverage values for about 30 platelets from each of the Silver #4 and Silver #6 samples are plotted in **Figure 16** as a function of the depth below the surface. Both of these systems show a transition from platelets with a fractional coverage of 0.0 to a fractional coverage of 1.0 with depth. However, Silver #6, which had larger platelets, had a larger percentage of platelets with a fractional coverage in the range of 0.25-0.75. This suggests that if both of these systems were illuminated by diffuse light, Silver #6 would likely have a reduced lightness compared to Silver #4. A visual qualitative comparison between the two samples under diffuse illumination confirmed this behavior.

As a final comment, it is noted that a strict relationship between the fractional coverage of the platelets and the measured appearance of a paint system, which is usually conducted

with light incident at 45° to the surface, can only be made when the fractional coverage is computed for light incident at that same angle. We expect this fractional coverage to differ from the omni-directional fractional coverage due to path length complications and projected area differences at very shallow angles in the omni-directional case. However, it is noted that the data in Table 1 confirm that the measured lightness (L^*) at 15° OS was lower for Silver #6, than for Silver #4. This is consistent with the qualitative observations made under diffuse light.

6. Summary and Conclusions

In this study we confirm that platelet orientation is the major microstructural property of platelet/polymer paint systems that affects visual appearance across a range of formulations. Other microstructural properties, in addition to orientation, were found to significantly affect appearance through multiple reflection events. Multiple reflections are related to additional microstructural parameters associated with the density and spacing of the platelets, such as the size and frequency of the gaps between the platelets, and the coverage of platelets by other platelets. The relationship between platelet gaps and appearance has not been reported on previously and is of value to both color designers and digital renderers. Because platelet gaps and multiple reflections significantly affect appearance, their inclusion in predictive models or digital rendering software is necessary to insure accurate results.

Digital rendering tools that do not incorporate both primary and secondary scattering events from platelet-containing materials risk overestimating the amount of near-specular scattered light. Other applications such as devices that utilize tiny mirrors such as a digital micro-mirror devices (DMD) [53], where individual mirrors can be addressed and assigned an

orientation to produce macroscopic images may benefit from a clearer understand of the link between microstructure and light scattering as well. This link cannot be limited to surface microstructure and must incorporate the entire 3D microstructure of the scattering layer to create a model or simulation based on the structure-property relationship of the scattering system.

Table 1: Formulation (as provided by supplier, where appropriate), application, and measurement details for the ten prepared silver samples. The target for the clearcoat and basecoat thicknesses for all samples was 50 μm and 20 μm, respectively.

Sample Name	Pigment: Binder Mass Ratio	Approx. Platelet Volume Fraction	Median Platelet Diameter (μm)	Average Platelet Thickness (μm)	L^* @ 15° OS (θ_{OUT}=30°)	Median Orientation Angle from microscopy (degrees)	RMS_{Error} (CDF%)	Gap Factor (gap size per unit sample length)	Application Method[54]
Silver #1	0.18	7.6%	17 ± 0.5	0.55 ± 0.02	143.3 ± 0.3	4.1 ± 0.4	0.02 ± 0.01	0.26 ± 0.01	Electrostatic Bell, Low Fluid Flow (90 cc/min)
Silver #2	0.18	7.6%	17 ± 0.5	0.55 ± 0.02	129.0 ± 0.3	5.3 ± 0.3	0.05 ± 0.02	0.32 ± 0.01	Electrostatic Bell, High Fluid Flow (210 cc/min)
Silver #3	0.18	7.6%	17 ± 0.5	0.55 ± 0.02	137.2 ± 0.3	4.0 ± 0.3	0.04 ± 0.02	0.33 ± 0.01	Electrostatic Bell, Nominal Fluid Flow (150 cc/min)
Silver #4	0.32	12.1%	25 ± 0.75	0.66 ± 0.03	130.2 ± 0.3	4.2 ± 0.3	0.03 ± 0.01	0.26 ± 0.01	Electrostatic Bell
Silver #5	0.11	4.4%	18.5 ± 0.56	0.58 ± 0.03	114.6 ± 0.3	5.3± 0.4	0.06 ± 0.01	0.31 ± 0.01	Electrostatic Bell
Silver #6	0.10	4.0%	11.5 ± 0.35	0.63 ± 0.03	108.3 ± 0.3	4.9 ± 0.3	0.10 ± 0.01	0.35 ± 0.01	Electrostatic Bell
Silver #7	0.19	7.6%	17 ± 0.5	0.61 ± 0.03	144.8 ± 0.3	3.1 ± 0.2	0.08 ± 0.02	0.16 ± 0.01	Spray gun
Silver #8	0.09	4.0%	17 ± 0.5	0.61 ± 0.03	119.2 ± 0.3	5.1 ± 0.4	0.06 ± 0.02	0.36 ± 0.01	Spray gun
Silver #9	**0.05**	**2.0%**	17 ± 0.5	0.61 ± 0.03	101.3 ± 0.3	6.4 ± 0.3	0.05 ± 0.02	0.30 ± 0.01	Spray gun
Silver #10	**0.02**	**1.0%**	17 ± 0.5	0.61 ± 0.09	87.5 ± 0.3	7.0 ± 0.4	0.0540 ± 0.017	0.30 ± 0.01	Spray gun

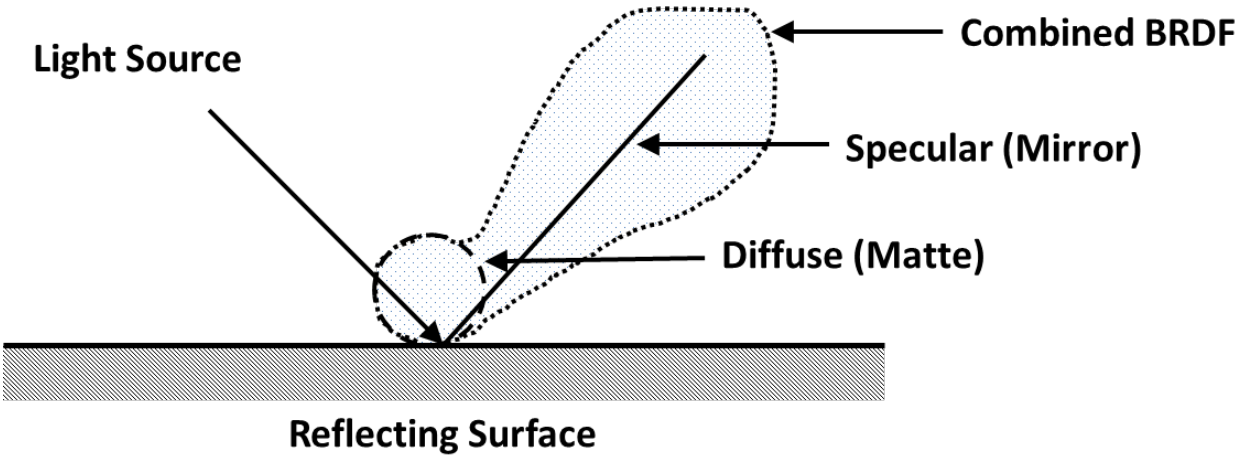

Figure 1: Schematic of different BRDFs that result from perfectly specular, diffuse specular, and diffuse surfaces. Also illustrated is a combined BRDF for a surface that consists of all three types of reflections.

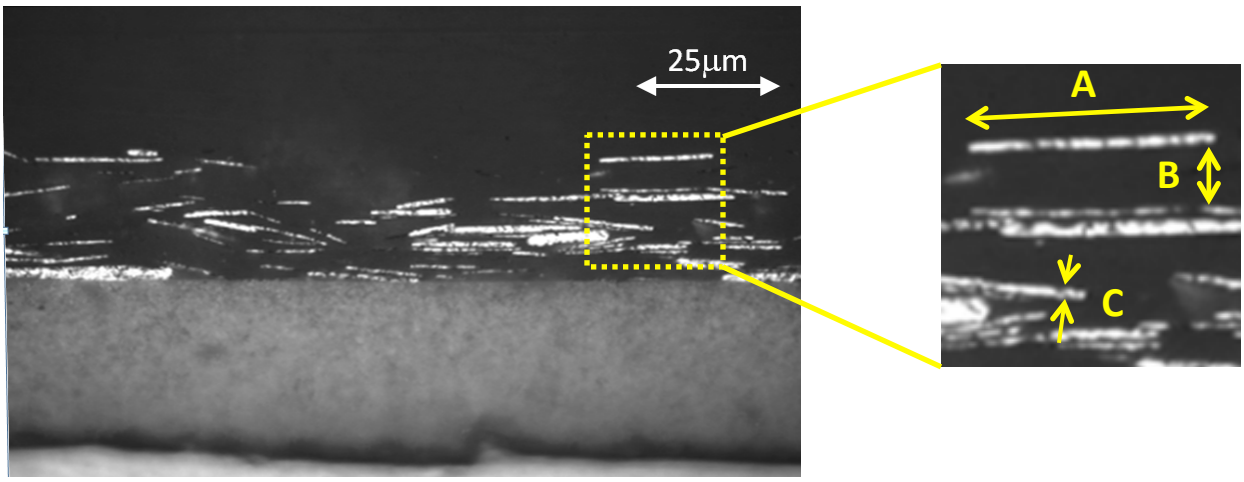

Figure 2: Cross-sectional view of typical silver basecoat system (Silver #1) taken with optical microscopy. The magnified view (25µm x 25µm) shows the platelet diameter (A), the gap size (B), and the platelet thickness (C).

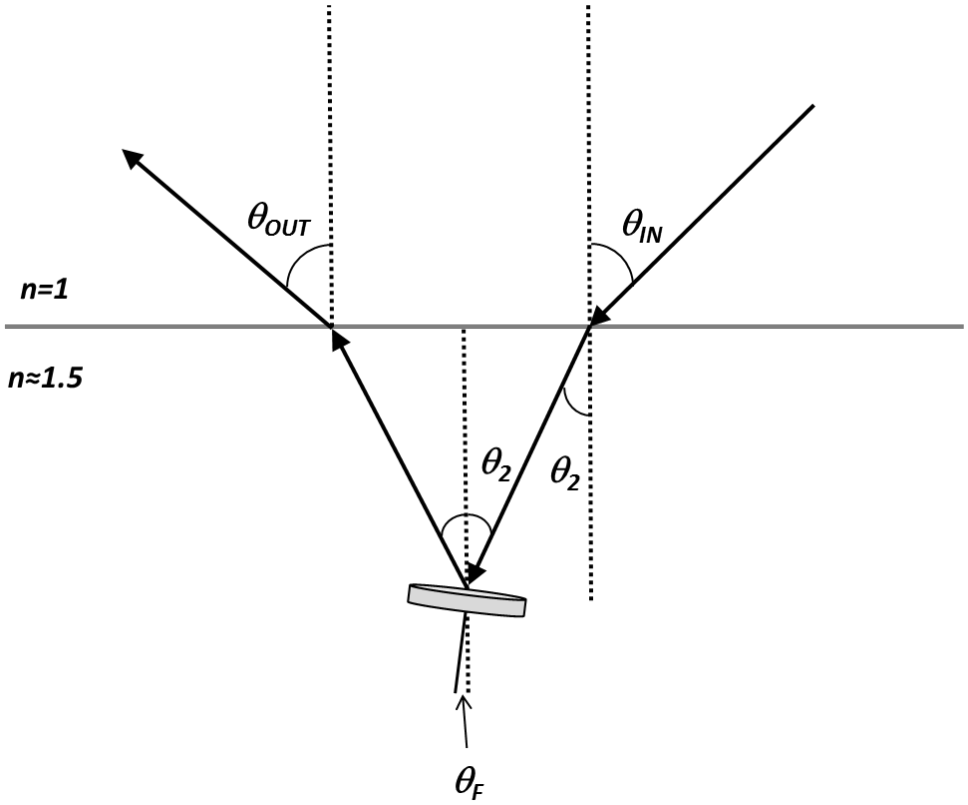

Figure 3: A schematic figure illustrating a single reflection from a metallic platelet in a paint system. Incident light enters the system at an angle of θ_{IN}. The light is then refracted by the air-clearcoat interface to a new angle (θ_2). The light progresses through the clearcoat layer until it reflects off of a platelet—in this case, the platelet face. The angle from normal of the platelet (θ_F) will determine the angle that the light intersects the air-clearcoat interface. This refraction will lead to the ray's exit angle of θ_{OUT}. This ray propagation is only true for single reflection, face reflections. If the ray strikes more than one platelet, a platelet edge, or the primer layer below, the ray will follow a different propagation path.

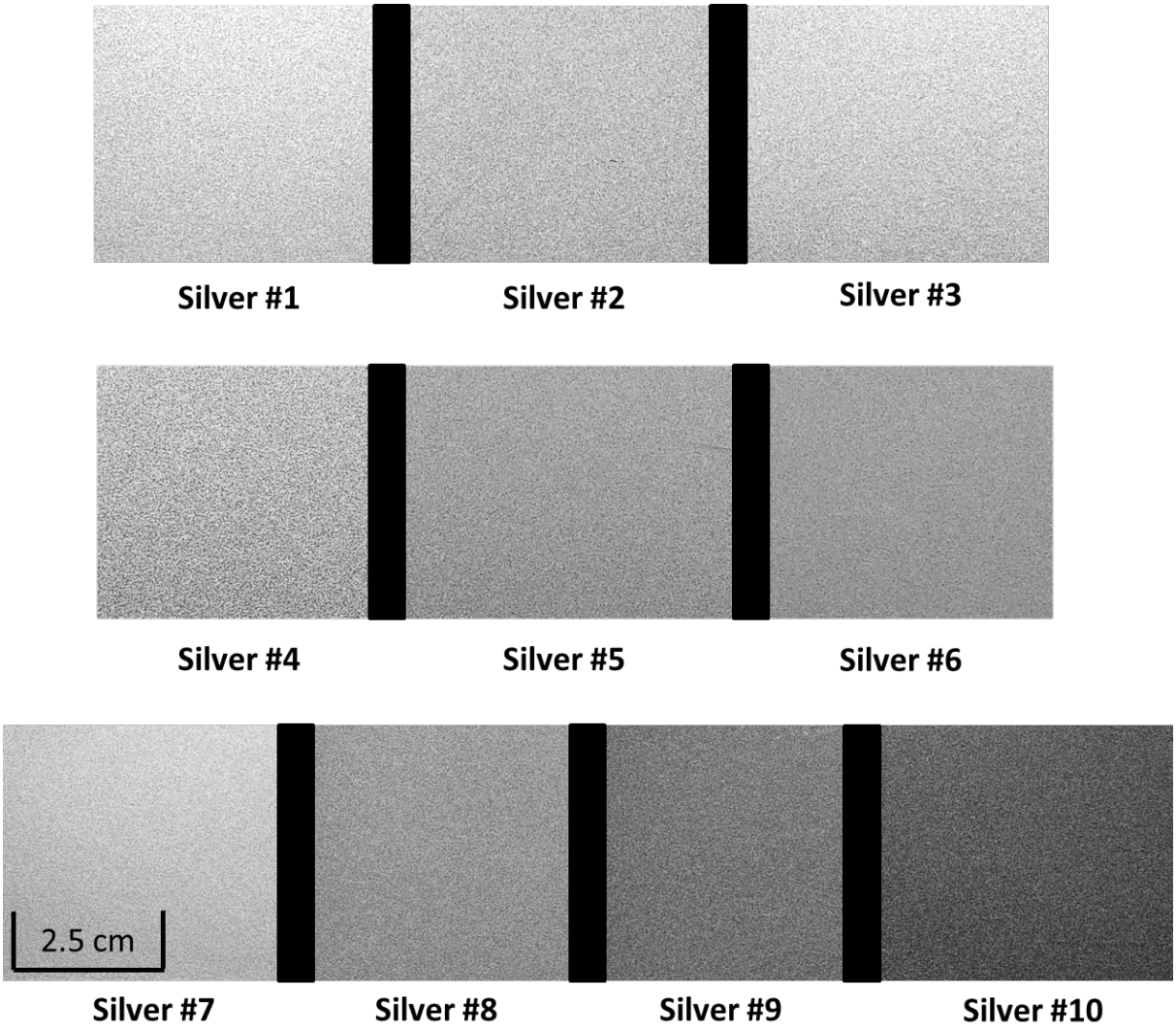

Figure 4: Digital images taken of each silver sample under study. Samples were imaged at 15° OS under daylight illumination from a MacBeth light booth. Silver #1-Silver #3 were applied under different process conditions. Silver #4-Silver #6 were formulated with different platelet sizes. Silver #7-Silver #10 were formulated with different volume fractions of like platelets. Measured lightness values for each sample are listed in Table 1.

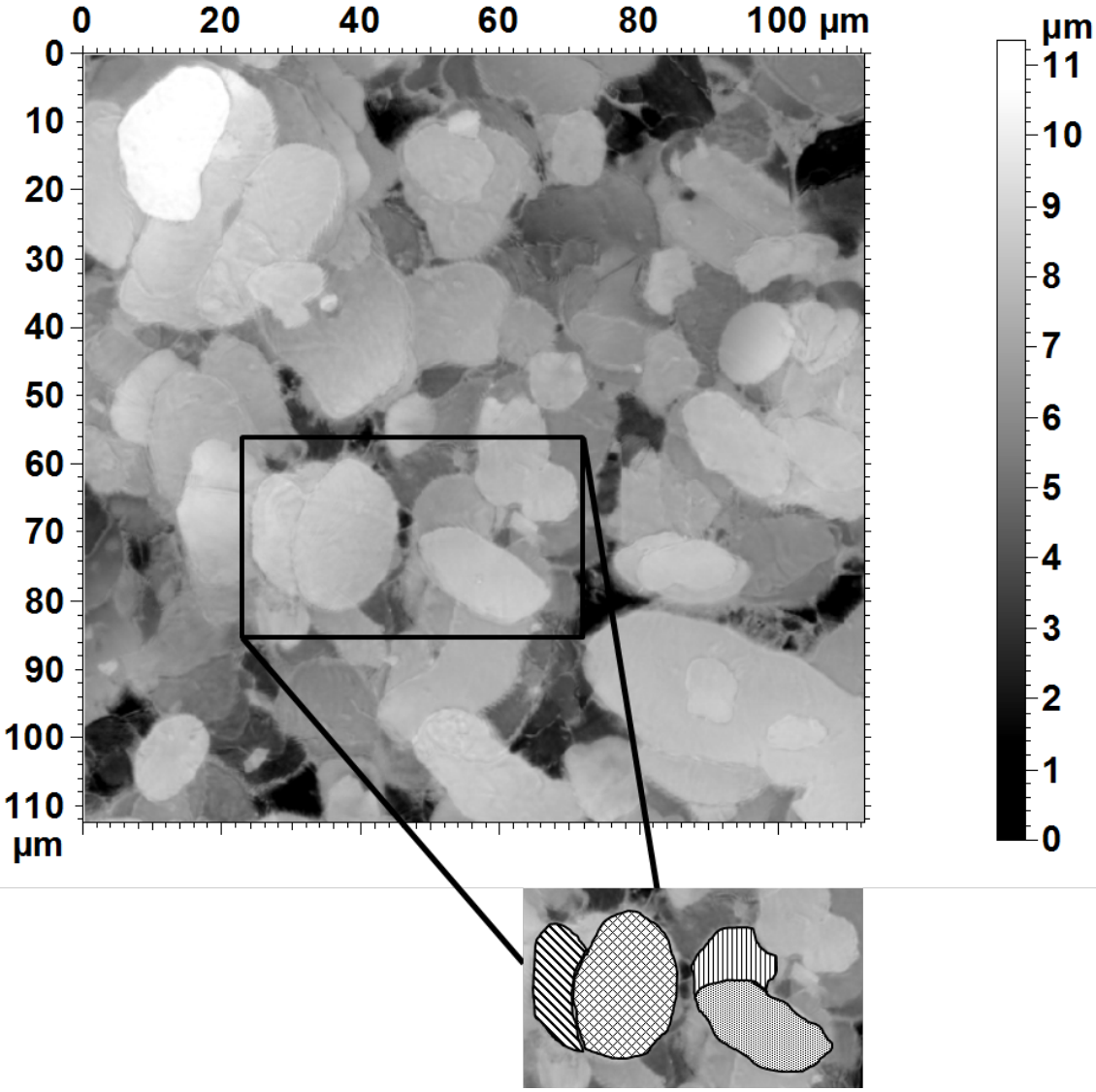

Figure 5: A height map for the Silver #1 sample obtained from laser-scanning-confocal microscopy. LSCM can only image platelet directly viewable from the surface normal direction. Many platelets are partially shadowed by other platelets. The visible area of some example individual platelet regions are highlighted in the callout. The angular data from each of these regions was weighted by each platelet's relative area to determine if this affected the match between the orientations produced by scattering and LSCM.

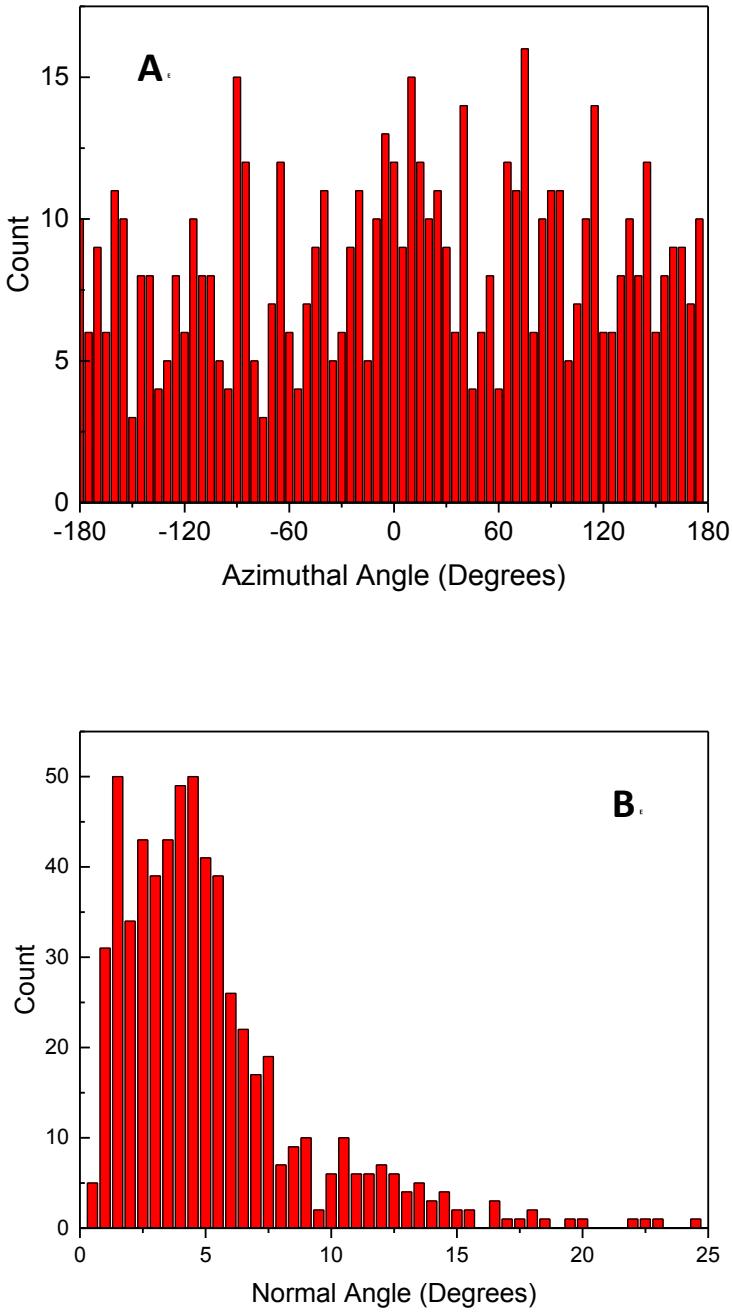

Figure 6: (A) Azimuthal angle counts (bin size of 5°) measured for Silver #1. The azimuthal angle data showed no obvious trend or bias. As a result, the azimuthal angle was assumed to be random. (B) Normal angle counts (bin size of 0.5°) measured for Silver #1. The normal angle does have a clear bias and distribution, with a maximum frequency of ~5°. The exact shape of this distribution varied slightly from sample to sample. It was this variation that was partially responsible for lightness variations between the samples.

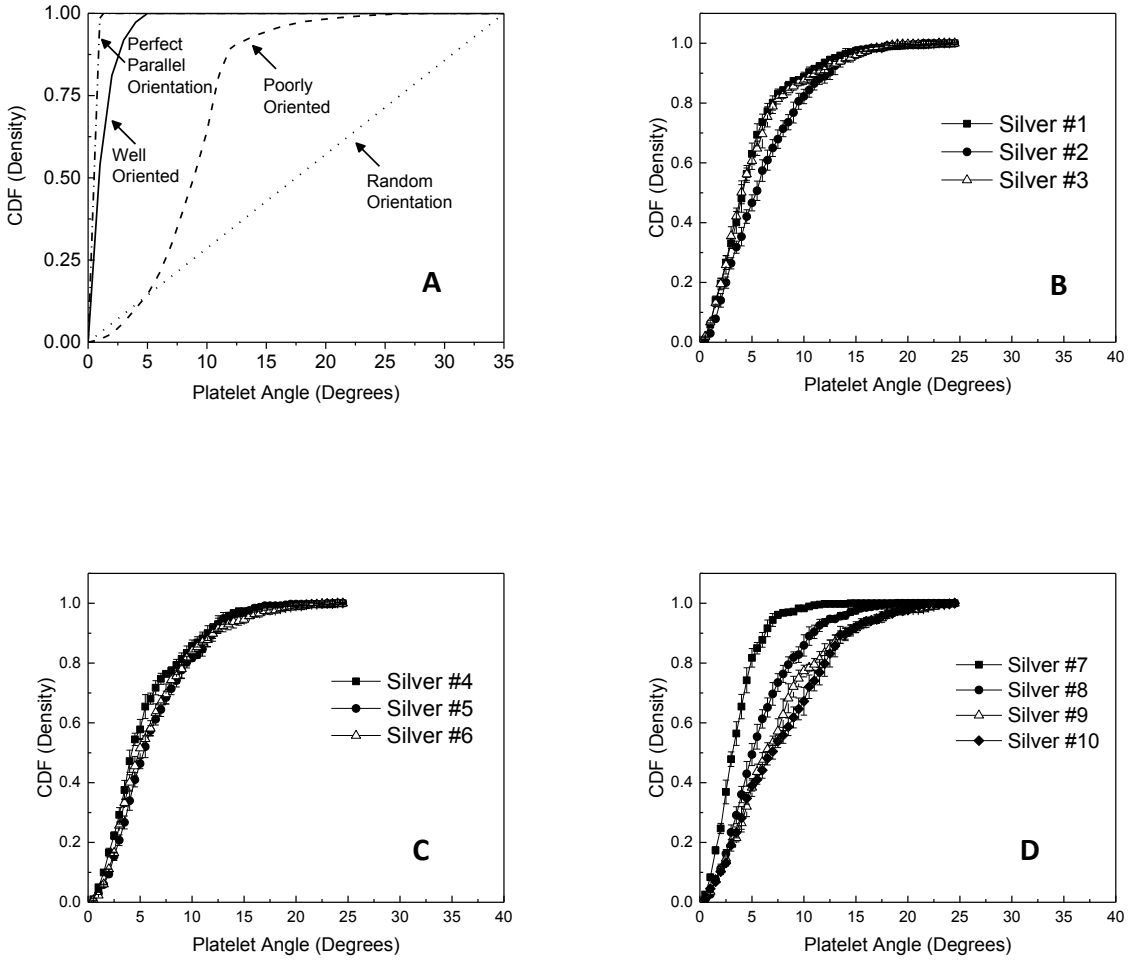

Figure 7: (A) The expected cumulative-density functions (CDFs) for perfectly oriented, well oriented, poorly oriented, and randomly oriented platelet systems. (B-D) Measured CDFs for the orientation for each paint system, as determined from LSCM observations.

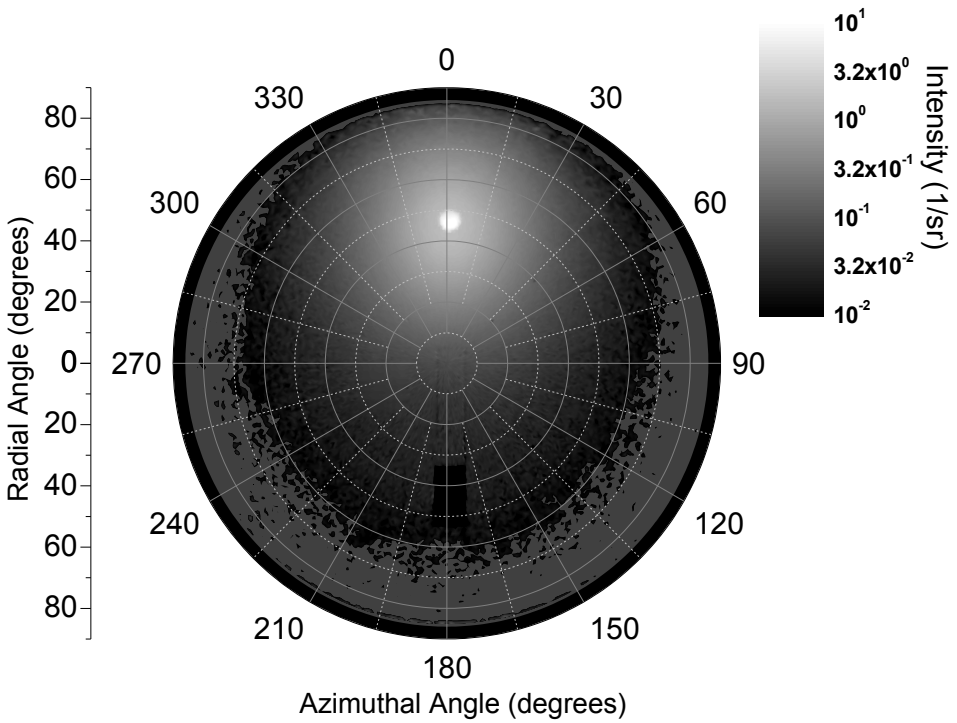

Figure 8: A spherical contour plot of scattered intensity from Silver #1. Incident light enters from a radial angle of 45° and an azimuthal angle of 180°. The scattered intensity focused around the specular direction and decreases rapidly away from specular.

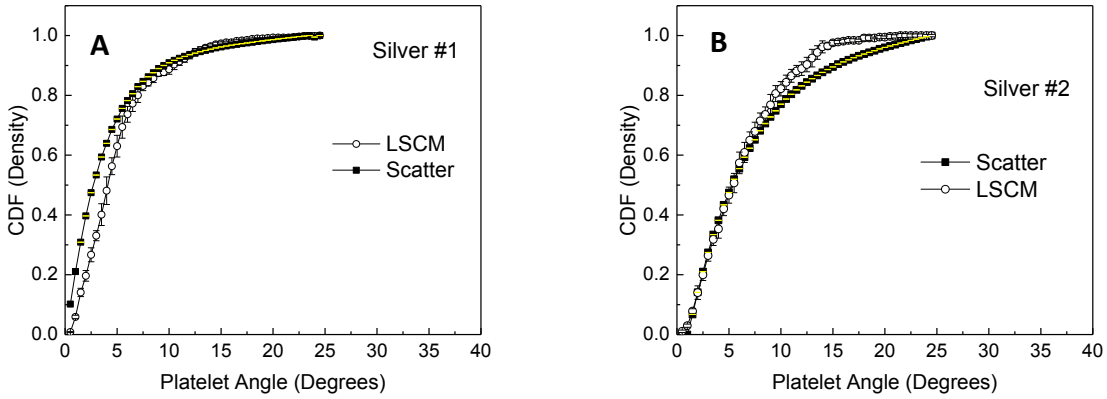

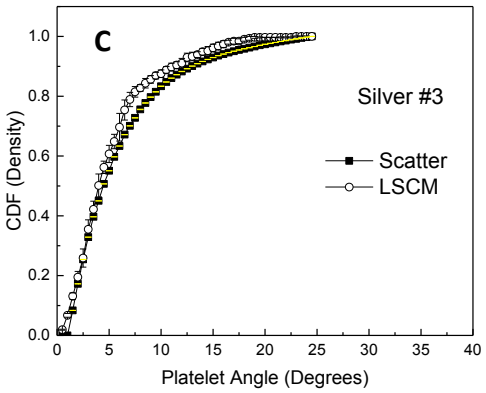
C
Silver #3
Scatter
LSCM
CDF (Density)
Platelet Angle (Degrees)

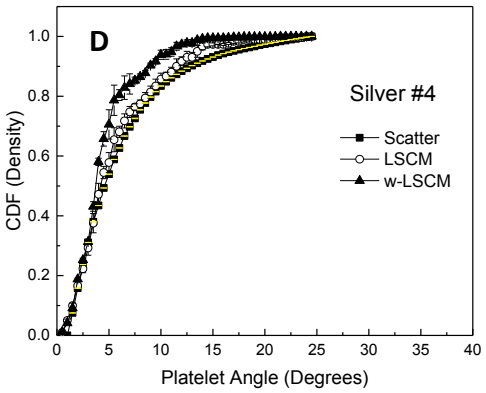
D
Silver #4
Scatter
LSCM
w-LSCM
CDF (Density)
Platelet Angle (Degrees)

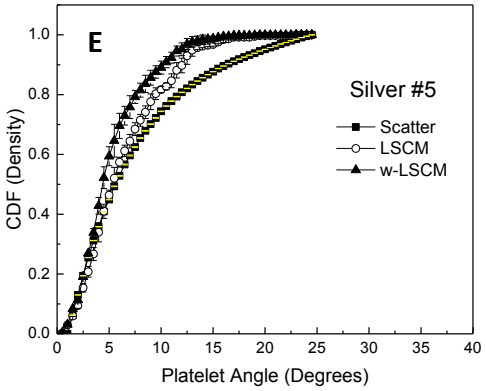
E
Silver #5
Scatter
LSCM
w-LSCM
CDF (Density)
Platelet Angle (Degrees)

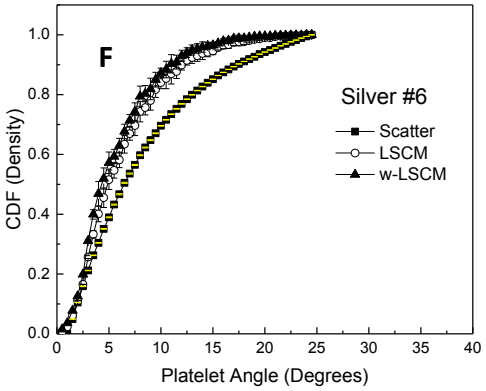
F
Silver #6
Scatter
LSCM
w-LSCM
CDF (Density)
Platelet Angle (Degrees)

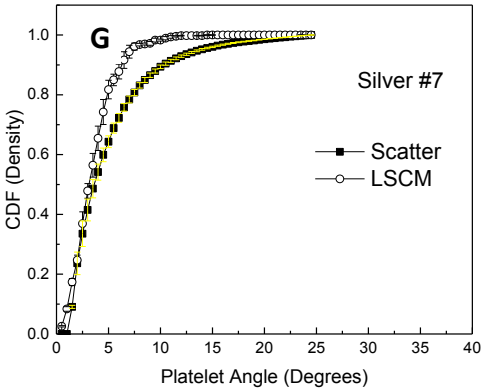
G
Silver #7
Scatter
LSCM
CDF (Density)
Platelet Angle (Degrees)

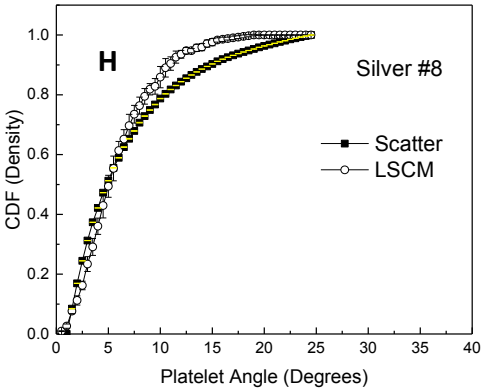
H
Silver #8
Scatter
LSCM
CDF (Density)
Platelet Angle (Degrees)

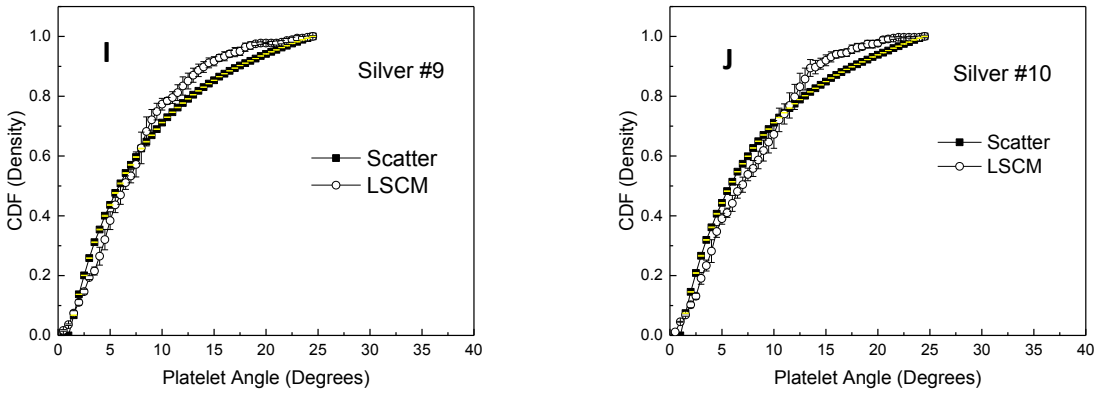

Figure 9: Comparisons between the distributions of the platelet orientations determined by confocal microscopy experiments (LCSM) and the distributions inferred from the scattering measurements (Scatter). Weighted LSCM profiles, as discussed in the text, have been added to the plots (d) through (f).

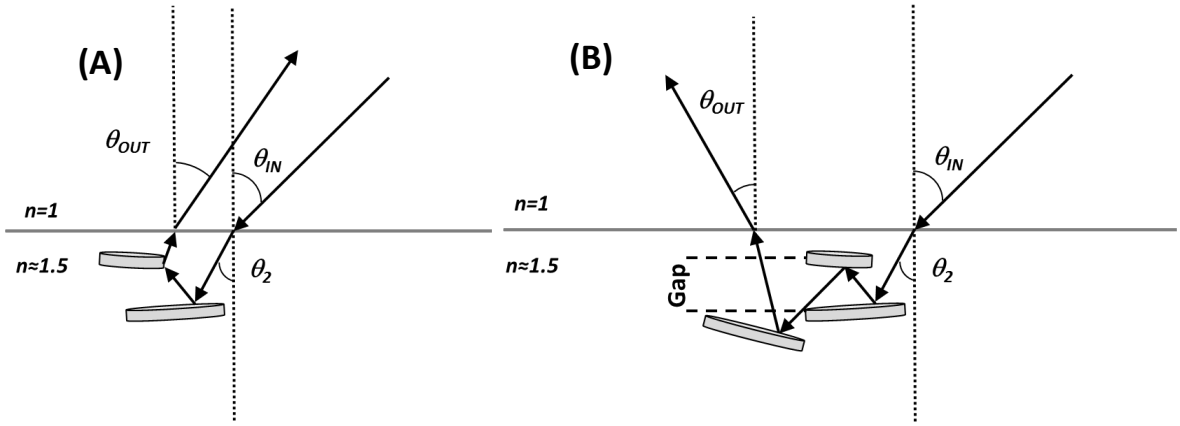

Figure 10: (A) Schematic illustration of a reflection from the edge of a platelet. (B) Schematic illustration of multiple reflections between platelets. In both cases, one can no longer infer orientation from scattering data, as that inference assumes single reflections off of platelet faces. Edge reflections and multiple reflection events will affect different regions of the scattering profile in different ways. Edge reflections contribute to the backscattered region while multiple reflection events contribute to the forward scattering region.

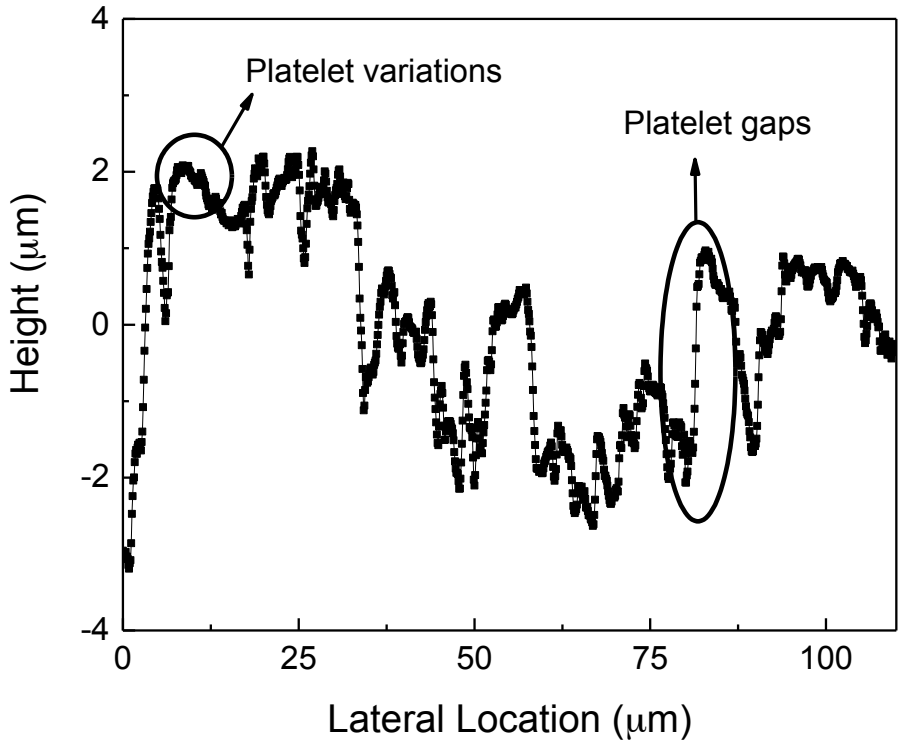

Figure 11: 2-D line-scan profile taken from the LSCM height map for Silver #1 shown in Figure 3. Small variations in the height are associated with variations along the surface of a single platelet, while large variations in height are associated with gaps between platelets.

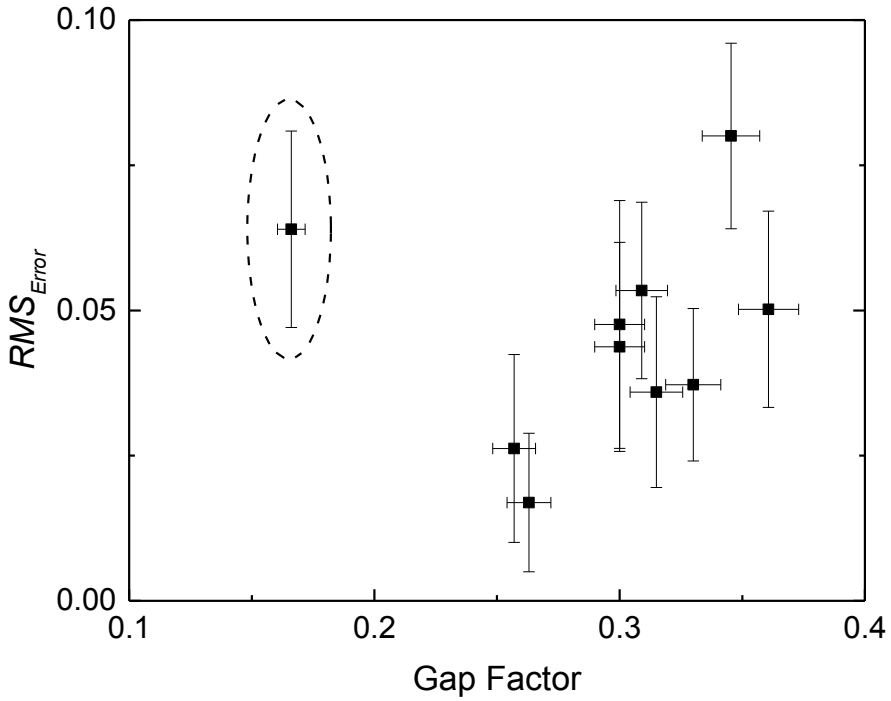

Figure 12: A plot of the RMS_{error} against the gap factor (defined in Section 4.3.1) for all ten samples. The circled datum point is from Sample #7, which was the most oriented sample of the series. On-going work is investigating whether there is any systematic effects on the relationship between the gap factor and the RMS_{error} for highly-oriented systems, or whether these are just a break-down in any apparent correlation.

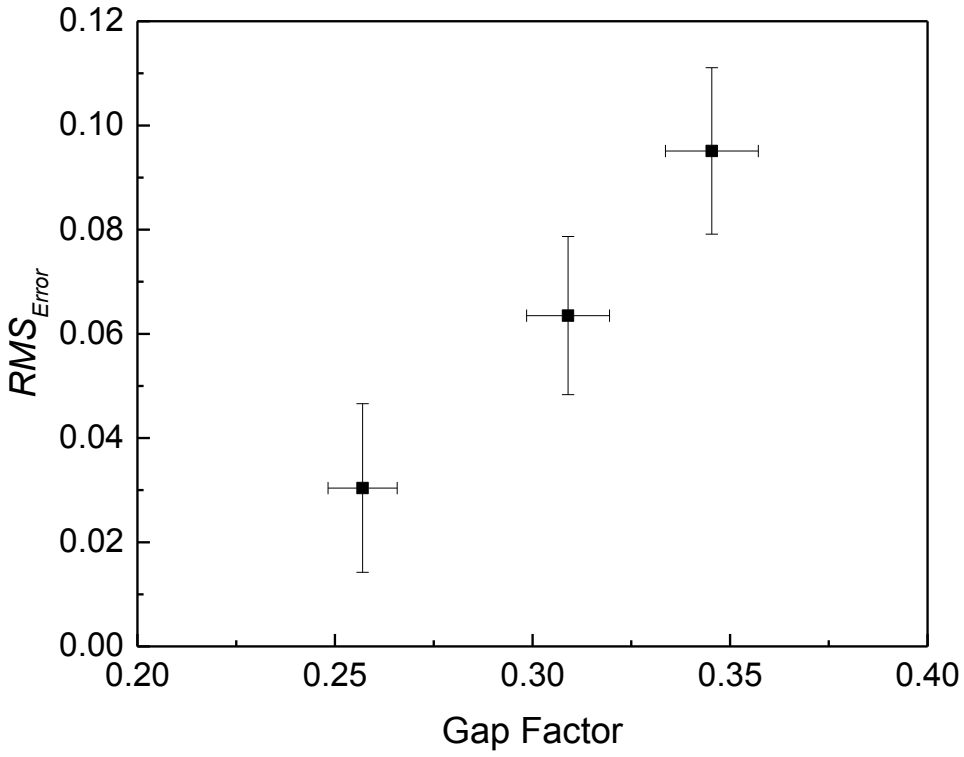

Figure 13: An apparent correlation between the RMS_{error} and the gap factor for a set of paint systems in which the platelets have similar orientations (Silver #4, Silver #5 and Silver #6).

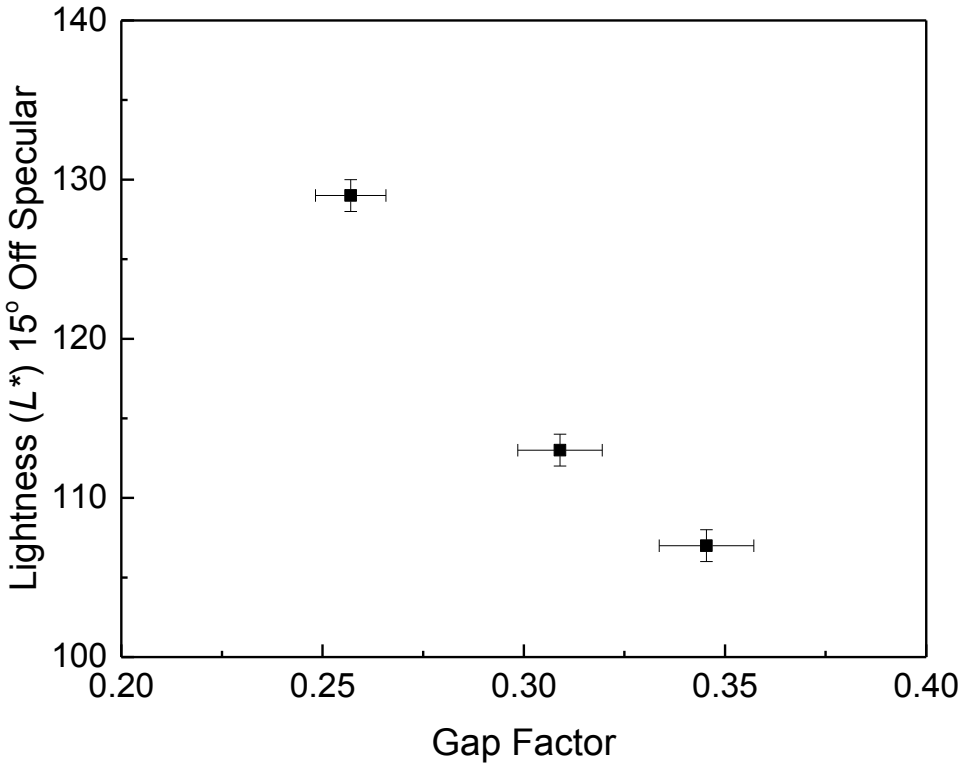

Figure 14: The correlation between the *L and gap factor for the samples identified as Silver #4, Silver #5 and Silver #6.**

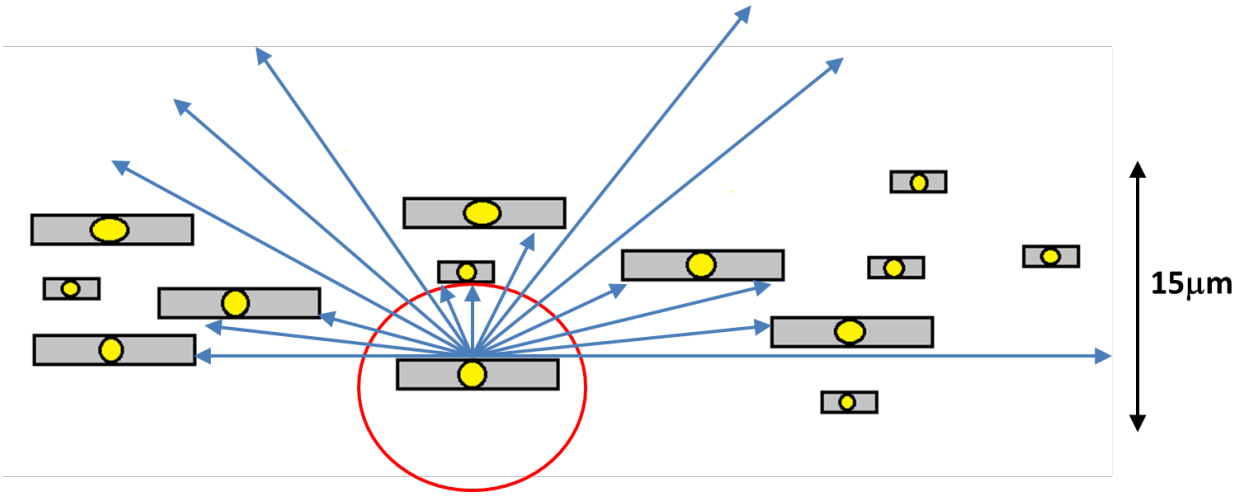

Figure 15: A schematic illustration of the modified pair-correlation analysis used to analyze the coverage of platelets. In this example, the platelet being considered has a fractional coverage of 0.3.

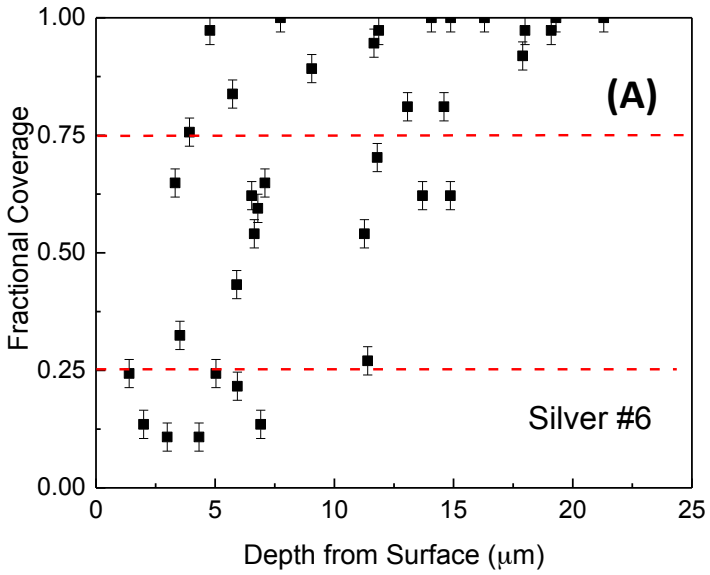

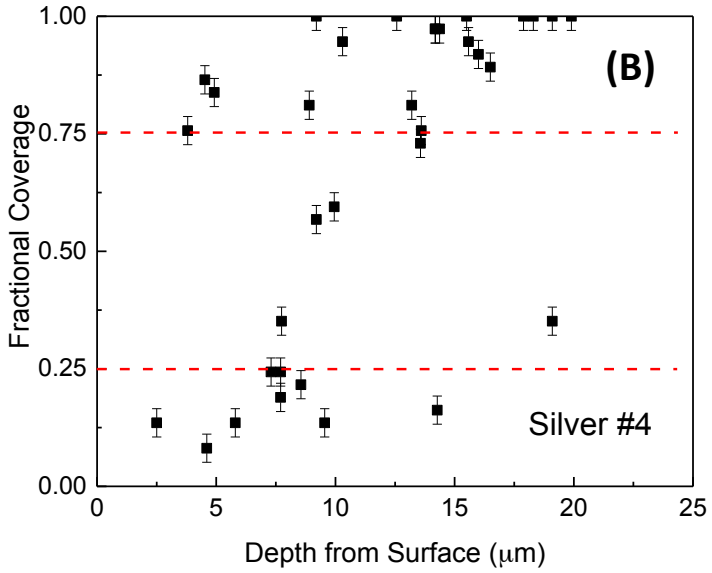

Figure 16: Plot of the coverage for individual platelets as a function of depth below the surface for (A) Silver #6, with a median platelet diameter of 11.5 μm, and (B) Silver #4, with a median platelet diameter of 25 μm. The system with the smaller platelets has more platelets with a fractional coverage between 0.25 and 0.75 than the other system. It is postulated that this is associated with a higher incidence of multiple reflections, which resulted in a reduced lightness observed in a diffuse illumination environment for Silver #6.

References

1. Haber RN, Hershenson M (1973) The psychology of visual perception. Holt, Rinehart & Winston, New York.
2. Mikec V (2005) Which parameters have an influence on customer's perception? What measurements on the car body?, SURCAR Conference.
3. Creusen ME, Schoormans JP (2005) The different roles of product appearance in consumer choice*. J Prod Innovation Manage 22:63-81.
4. Andrews D, Nieuwenhuis P, Ewing PD (2006) Black and beyond—colour and the mass-produced motor car. Optics & Laser Technology 38:377-391.
5. Dawar N, Parker P (1994) Marketing universals: Consumers' use of brand name, price, physical appearance, and retailer reputation as signals of product quality. The Journal of Marketing 58:81-95.
6. Nichols ME (2012) The Modeling and Rendering of Complex Automotive Paint. American Coatings Association Transportation Conference.
7. Schanda J (2007) Colorimetry: Understanding the CIE system. John Wiley & Sons, Hoboken.
8. McLaren K (1976) XIII–The development of the CIE 1976 (*L* a* b**) uniform colour space and colour‐difference formula. Journal of the Society of Dyers and Colourists 92:338-341.
9. Robertson AR (1990) Historical development of CIE recommended color difference equations. Color Research & Application 15:167-170.
10. Wyszecki G, Stiles WS (1982) Color science. Wiley, New York.
11. Olson GB (1997) Computational design of hierarchically structured materials. Science 277:1237-1242.
12. Nørskov JK, Bligaard T, Rossmeisl J, Christensen CH (2009) Towards the computational design of solid catalysts. Nature chemistry 1:37-46.
13. Curtarolo S, Hart GL, Nardelli MB, Mingo N, Sanvito S, Levy O (2013) The high-throughput highway to computational materials design. Nature materials 12:191-201.
14. Nicodemus FE (1965) Directional reflectance and emissivity of an opaque surface. Appl Opt 4:767-773.
15. Ashikhmin M, Premoze S (2007) Distribution-based brdfs. Unpublished Technical Report, University of Utah 2.
16. Medina JM, Díaz JA (2013) Characterization of reflectance variability in the industrial paint application of automotive metallic coatings by using principal component analysis. Optical Engineering 52:051202.
17. Seo MK, Kim KY, Kim DB, Lee KH (2011) Efficient representation of bidirectional reflectance distribution functions for metallic paints considering manufacturing parameters. Optical Engineering 50:013603.
18. Ershov S, Kolchin K, Myszkowski K (2001) Rendering Pearlescent Appearance Based On Paint‐Composition Modelling. EUROGRAPHICS 2001 20:227-238.
19. Germer TA, Nadal ME (2001) Modeling the appearance of special effect pigment coatings. International Symposium on Optical Science and Technology 1:77-86.
20. Cook RL, Torrance KE (1982) A reflectance model for computer graphics. ACM Transactions on Graphics (TOG) 1:7-24.

21. Weidlich A, Wilkie A (2007) Arbitrarily layered micro-facet surfaces. Proceedings of the 5th international conference on Computer graphics and interactive techniques in Australia and Southeast Asia. ACM 1:171-178.
22. Rump M, Müller G, Sarlette R, Koch D, Klein R (2008) Photo-realistic Rendering of Metallic Car Paint from Image Based Measurements. Computer Graphics Forum 27:527-536.
23. Germer TA, Marx E (2004) Ray model of light scattering by flake pigments or rough surfaces with smooth transparent coatings. Appl Opt 43:1266-1274.
24. Sung L, Nadal ME, McKnight ME, Marx E, Laurenti B (2002) Optical reflectance of metallic coatings: effect of aluminum flake orientation. J Coatings Technol 74:55-63.
25. Kettler W, Richter G (1997) Investigation on topology of platelet-like effect-pigments in automotive surface-coatings. Progress in organic coatings 31:297-306.
26. Klein GA, Meyrath T (2010) Industrial color physics. Springer, New York.
27. McCamy C (1996) Observation and measurement of the appearance of metallic materials. Part I. Macro appearance. Color Research & Application 21:292-304.
28. Maile FJ, Pfaff G, Reynders P (2005) Effect pigments—past, present and future. Progress in Organic Coatings 54:150-163.
29. Rodrigues A (2004) Color technology and paint. Color and Paints Interim Meeting of the International Color Association Proceedings 1:103-108.
30. Pfaff, G. (2001) Special Effect Pigments. High Performance Pigments (ed H. M. Smith), Wiley-VCH Verlag GmbH & Co. KGaA, Weinheim, FRG.
31. Lambourne R, Strivens T (1999) Paint and surface coatings: theory and practice. Elsevier, West Sussex.
32. Levinson R, Berdahl P, Akbari H (2005) Solar spectral optical properties of pigments—Part I: model for deriving scattering and absorption coefficients from transmittance and reflectance measurements. Solar Energy Mater Solar Cells 89:319-349.
33. Gunde MK, Orel ZC (2000) Absorption and scattering of light by pigment particles in solar-absorbing paints. Appl Opt 39:622-628.
34. Tachi K, Okuda C, Suzuki S (1990) Mechanism of aluminum flake orientation in metallic topcoats. Journal of coatings technology 62:43-50.
35. Thouless M, Dalgleish B, Evans A (1988) Determining the shape of cylindrical second phases by two-dimensional sectioning. Materials Science and Engineering: A 102:57-68.
36. Bandyopadhyay J, Malwela T, Ray SS (2012) Study of change in dispersion and orientation of clay platelets in a polymer nanocomposite during tensile test by variostage small-angle X-ray scattering. Polymer 53:1747-1759.
37. Yang C, Smyrl W, Cussler E (2004) Flake alignment in composite coatings. J Membr Sci 231:1-12.
38. Pelicon P, Klanjšek-Gunde M, Kunaver M, Simcic J, Budnar M (2002) Analysis of metallic pigments by ion microbeam. Nuclear Instruments and Methods in Physics Research Section B: Beam Interactions with Materials and Atoms 190:370-374.
39. Gunde MK, Kunaver M, Mozetic M, Pelicon P, Simcic J, Budnar M, Bele M (2002) Microstructure analysis of metal-effect coatings. Surface Coatings International Part B: Coatings Transactions 85:115-121.

40. Kirchner E, Houweling J (2009) Measuring flake orientation for metallic coatings. Progress in organic coatings 64:287-293.
41. Pauli H (1976) Proposed extension of the CIE recommendation on “Uniform color spaces, color difference equations, and metric color terms”. JOSA 66:866-867.
42. Wright WD (1929) A re-determination of the trichromatic coefficients of the spectral colours. Transactions of the Optical Society 30:141-164.
43. Guild J (1932) The colorimetric properties of the spectrum. Philosophical Transactions of the Royal Society of London.Series A, Containing Papers of a Mathematical or Physical Character 1:149-187.
44. Kasarova SN, Sultanova NG, Ivanov CD, Nikolov ID (2007) Analysis of the dispersion of optical plastic materials. Optical Materials 29:1481-1490.
45. Di Domenico J, Henshaw P (2012) The effects of basecoat bell application parameters on elements of appearance for an automotive coatings process. Journal of Coatings Technology and Research 9:675-686.
46. Ellwood KR, Tardiff JL, Alaie SM (2014) A simplified analysis method for correlating rotary atomizer performance on droplet size and coating appearance. Journal of Coatings Technology and Research 11:303-309.
47. Beckmann P, Spizzichino A (1987) The scattering of electromagnetic waves from rough surfaces. Artech House, Inc., Norwood.
48. Bartl J, Baranek M (2004) Emissivity of aluminum and its importance for radiometric measurement. Measurement of Physical Quantities 43:31-36.
49. De Podesta M (2002) Understanding the properties of matter. CRC Press, Boca Raton.
50. Waisman E (1973) The radial distribution function for a fluid of hard spheres at high densities: mean spherical integral equation approach. Molecular Physics 25:45-48.
51. Yuste SB, Santos A (1991) Radial distribution function for hard spheres. Physical Review A 43:5418-5423.
52. Kincaid J, Weis J (1977) Radial distribution function of a hard-sphere solid. Mol Phys 34:931-938.
53. Younse JM (1993) Mirrors on a chip. Spectrum, IEEE 30:27-31.
54. Streitberger HJ, Kreis W, Decher G Schlenoff JB (2005) Automotive paints and coatings. VCH Verlag GmbH & Co. KGaA, Weinheim, FRG.